Lawrence Livermore National Laboratory

2013 LLNL Nuclear Forensics Summer Program

Glenn T. Seaborg Institute
Lawrence Livermore National Laboratory
Physical and Life Sciences
Livermore, CA 94550

Director: Annie Kersting (kersting1@llnl.gov)
Administrator: Camille Vandermeer
Website: https://seaborg.llnl.gov/

Sponsors:
National Technical Nuclear Forensics Center, Domestic Nuclear Detection Office, Department of Homeland Security
LLNL: Glenn T. Seaborg Institute, Physical and Life Sciences Directorate

Lawrence Livermore National Laboratory is operated by Lawrence Livermore National Security, LLC, for the U.S. Department of Energy, National Nuclear Security Administration under Contract DE-AC52-07NA27344.

LLNL-TR-644247

Disclaimer

Auspices

This work was performed under the auspices of the U.S. Department of Energy by Lawrence Livermore National Laboratory under Contract DE-AC52-07NA273

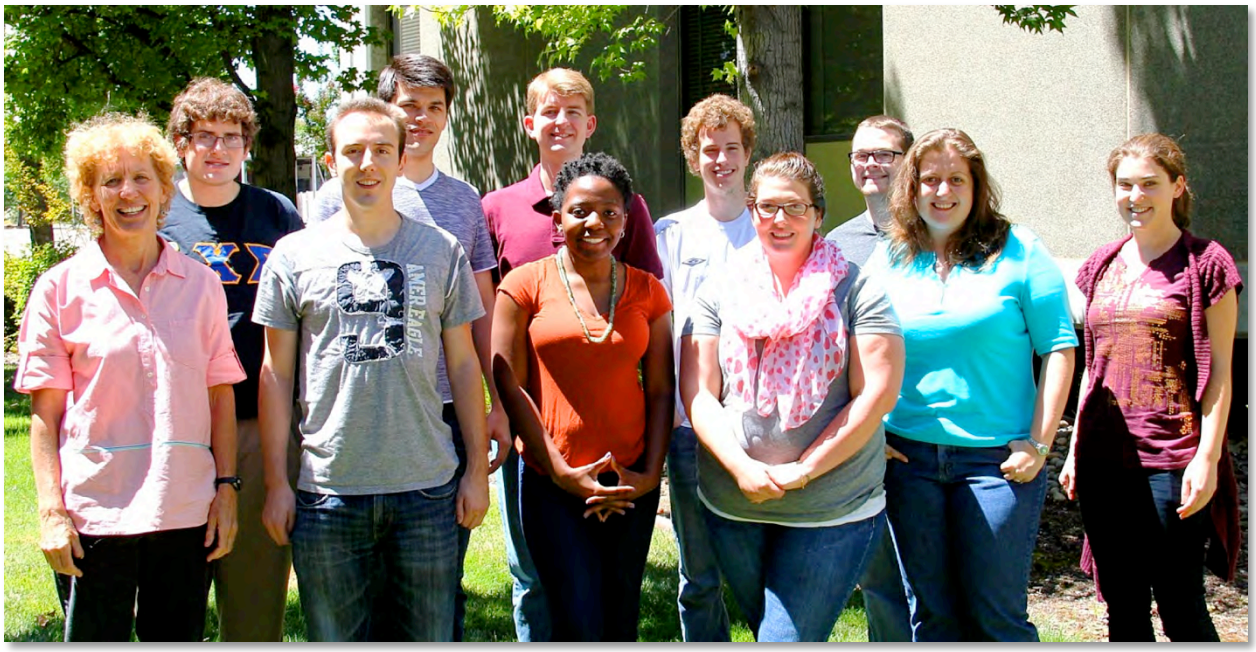

Figure 1. Annie Kersting, Director, Glenn T. Seaborg Institute (far left), and 2013 Nuclear Forensics Summer Program Students

The Lawrence Livermore National Laboratory (LLNL) Nuclear Forensics Summer Program is designed to give both undergraduate and graduate students an opportunity to come to LLNL for 8–10 weeks for a hands-on research experience. Students conduct research under the supervision of a staff scientist, attend a weekly lecture series, interact with other students, and present their work in poster format at the end of the program. Students also have the opportunity to meet staff scientists one-on-one, participate in LLNL facility tours (e.g., the National Ignition Facility and Center for Accelerator Mass Spectrometry) to gain a better understanding of the multi-disciplinary, on going science at LLNL.

Currently called the Nuclear Forensics Summer Program, this program began 13 years ago as the Actinide Sciences Summer Program. The program is run within the Glenn T. Seaborg Institute in the Physical and Life Sciences Directorate at LLNL. The goal of the Nuclear Forensics Summer Program is to facilitate the training of the next generation of nuclear scientists and engineers to solve critical national security problems in the field of nuclear forensics and have the student experience conducting research at the Lab. We select students who are majoring in physics, chemistry, geology, mathematics, nuclear engineering, chemical engineering and environmental sciences. Students engage in research projects in the disciplines of actinide chemistry, radiochemistry, isotopic analysis, computational analysis, radiation detection, and nuclear engineering in order to strengthen the "pipeline" for future scientific disciplines critical to DHS (DNDO), NNSA.

This is a competitive program with over 80 applicants for the 7–10 slots available. Students come highly recommended from universities all over the country. For example, this year we hosted students from Texas A&M, University of Cincinnati, Washington State University, University of Nevada, Las Vegas, and University of Missouri. (See Table 1).

This year's students conducted research on such diverse topics as actinide (Np, U, Pu) isotopic fingerprinting, statistical modeling in nuclear forensics, actinide analysis for nuclear forensics, environmental radiochemistry, radiation detector materials development, coincidence counting methods, nuclear chemistry, and heavy element separations chemistry (see Table 2.) Graduate students are invited to return for a second year at their mentor's discretion. We encourage the continuation of research collaboration between graduate student, faculty advisor, and Laboratory scientists.

In addition to hands-on training, students attend a weekly lecture series on topics applicable to the field of nuclear forensics (see Table 3). Speakers are experts from both within LLNL and external to it. Speakers are able to discuss the importance of their work in the context of advances in the field of nuclear forensics.

Graduate and undergraduate students on fellowships such as the Nuclear Forensics Graduate Fellowship are invited into our summer program. They usually come for 12 weeks and can return the following summer or stay throughout the year depending on their research needs. This year we had five Nuclear Forensics Fellows, four in the graduate program and one in the undergraduate program (Table 1, noted by an asterisk).

We also host students who are participating in the DOE-sponsored "Summer School in Radiochemistry" course held at San Jose State University and have recruited from this program. They come for a day, meet our summer students, see the research our students are doing, and tour our facilities. Staff scientists also participate in the Nuclear Forensics Undergraduate Summer Program sponsored by DHS-DNDO (FY13 held at University of Nevada, Las Vegas). This year the students come to LLNL for two days to meet our summer students, learn about their research, meet the staff and learn more about work at a national laboratory.

We use our summer program to create a successful pipeline of top-quality students from universities across the U.S. Since 2002, 42 students have returned and/or conducted their graduate research at LLNL:

- 12 became postdoctoral fellows at LLNL.
- 3 became postdoctoral fellows at other national labs.
- 7 were hired as career scientists at LLNL.
- 3 were hired as career scientists at other national labs.
- 3 were hired as faculty in the area of nuclear forensics/radiochemistry/nuclear science.

A big factor in the success of this program is the dedication of the staff scientists who volunteer to mentor the summer students. In FY13, funding from the Nuclear Forensics Graduate Mentoring Program (sponsor: DNDO) helped to partially support the time staff took to teach the summer interns. Staff scientists were able to take the necessary time to develop an appropriate summer project for their student, oversee necessary safety training, and dedicate more time to helping the interns maximize their productivity and scientific potential.

The posters presented at our Laboratory Student Poster Day are included at the end of this report. Two of our students won 'best poster' award out of about 250 poster presentations.

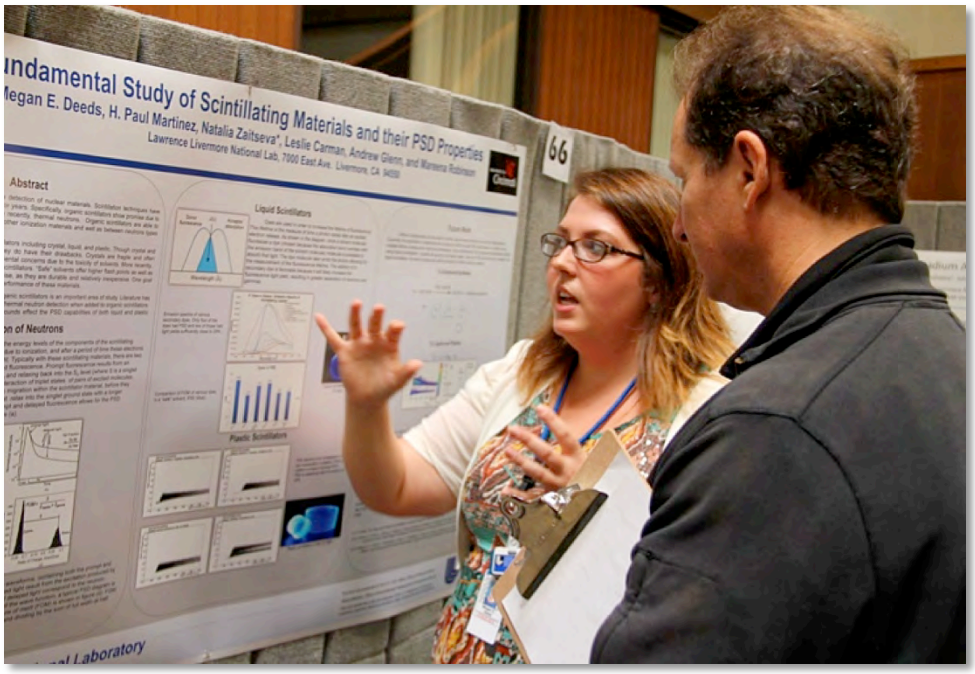
ndamental Study of Scintillating Materials and their PSD Properties
Megan E. Deeds, H. Paul Martinez, Natalia Zaitseva*, Leslie Carman, Andrew Glenn, and Marrena Robinson
Lawrence Livermore National Lab, 7000 East Ave. Livermore, CA 94550
Abstract
Liquid Scintillators
Plastic Scintillators
66


NOTICE

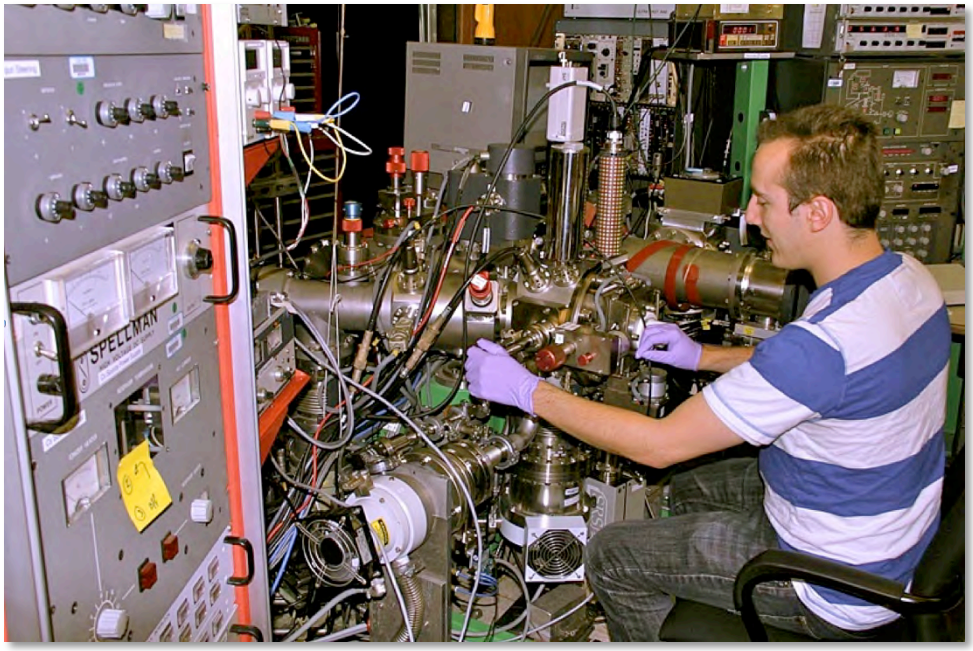
SPELLMAN


CLEMSON
Characterization of TBP using FTIR-ATR and Carbon Stable Isotopes
April R. Gillens[1], Michael Singleton[2], and Brian A. Powell[1]; [1]Environmental Engineering and Earth Sciences, Clemson University, Clemson, SC
[2]Environmental Radiochemistry Group, Chemical Sciences Division, Physical and Life Sciences Directorate, Lawrence Livermore National Laboratory, Livermore, CA
Research Objectives
TBP Degradation Mechanisms
Acidic Hydrolysis
vs.
FTIR-ATR Results
A.


ORTEC

Table 1. Summer Students

Student	Major	University	Year
Marisa Alfanso	Chemistry	Texas A&M University, College Station	Grad
Lucas Boron-Brenner	Radiochemistry	University of Nevada, Las Vegas	Grad
Megan Deeds	Chemistry	University of Cincinnati	Grad
Chad Durrant*	Nuclear Engineering	The Pennsylvania State University	Grad
Marc Fitzgerald*	Chemistry	University of Nevada, Las Vegas	Grad
April Gillens*	Environmental Engineering and Earth Sciences	Clemson University	Grad
Mitch Goshert	Chemistry	University of Missouri	Grad
Patrick Harms	Geology	Cal State University, East Bay	Grad
Corey Keith	Nuclear Engineering	Texas A&M University, College Station	Grad
Morgan Kelley	Radiochemistry	Washington State University	Grad
Jeff Rolfes*	Radiochemistry	University of Nevada, Las Vegas	Grad
Rodrigo Tapia**	Mathematics and Chemistry	University of Georgia	Undergrad

*= Nuclear Forensics Graduate Fellows
** = Nuclear Forensics Undergraduate Intern

Table 2. Student Projects and Mentors

Student	Mentor	Project
Marisa Alfanso	Dawn Shaughnessy	Analysis of Vanadium Activation Products from NIF Irradiations
Lucas Boron-Brenner	Gary Eppich	U Isotopic Measurements of Fallout Spherules Using Isotope Dilution Mass Spectrometry
Megan Deeds	Natalia Zaitzev	Fundamental Study of Scintillation Materials and their PSD Properties
Chad Durrant*	James Begg/ Mavrik Zavarin	Environmental Transport of Pu: Desorption of Pu in a Multi-Mineral System
Marc Fitzgerald*	Kim Knight	Spatially Resolved Analyses of Historical Fallout
April Gillens*	Mike Singleton	Characterization of TBP using FTIR-ATR and Carbon Stable Isotopes.
Mitch Goshert	Patrick Huang	Bonding and Redox Behavior in Actinide Coordination Complexes: First Principles
Patrick Harms	Brad Esser	Tritium and Stable Isotope Survey of California Surface Water
Corey Keith	Brian Bandong	High Energy Neutron Foil Activation for Davis Cals
Morgan Kelley	Jennifer Jo Ressler	Validation of a Phenomenological Fission Model.
Jeff Rolfes*	Roger Henderson	Development of a Chemical System for Rutherfordium
Rodrigo Tapia**	Brett Isselhardt	Using Computed Tomography to Non-Destructively Characterize Radioactive Fallout in 3D

* = Nuclear Forensics Undergraduate Intern
**= Nuclear Forensics Graduate Fellows

Table 3. Seminar Schedule

Date	Speaker	Topic
6/20/13	Dawn Shaughnessy Group Leader, Experimental Nuclear and Radiochemistry, Chemical Sciences Division	Superheavy Element Discovery at LLNL
6/27/13	Mona Dreicer Deputy Program Director for Nuclear and Domestic Security and Deputy Director of the Center for Global Security Research (CGSR)	Treaty Monitoring and Verification
7/3/13	Arthur Rodgers Scientist, Earth and Energy Division	Prompt Forensics with Speed-of-Sound Data
7/11/13	Stephan Friedrich Scientist, Physics Division	Superconducting Gamma Spectrometers with Ultra-high Energy Resolution for Nuclear Forensics
7/18/13	James Begg, Postdoc, Chemical Sciences Division Greg Brennecka, Postdoc, Chemical Sciences Division	Actinides in the Environment Geolocation of Nuclear Materials for Forensic Applications
7/25/13	Brett Isselhardt, Scientist, Chemical Sciences Division	Case Studies in Nuclear Forensics
8/1/13	Kim Budil N Program Manager, Nuclear Counterterrorism, Global Security Principal Directorate	A Journey Through the Nuclear Core: A Career at LLNL
8/8/13	Annie Kersting Director, Glenn T. Seaborg Institute, Physical and Life Sciences Directorate	Closing out the program

Analysis of Vanadium Activation Products from NIF Irradiations

Marisa Alfonso[1,2], Evgeny Tereshatov[1], John Despotopulos[1,3], Narek Gharibyan[1], Ken Moody[1], Dawn Shaughnessy[1]

[1]Lawrence Livermore National Laboratory, Chemical Sciences Division, PLS
[2]Texas A&M University [3]University of Nevada – Las Vegas

Background

National Ignition Facility (NIF) here at LLNL is a premier nuclear science facility. NIF has the capabilities of producing the world's largest neutron flux - 10^{15} particles. The instantaneous flood of neutrons makes it possible to measure nuclear reaction cross sections without having to correct for late-time neutron contributions, an issue with most other neutron sources. Also, NIF can be used to produce radioisotopes for nuclear forensics exercises.

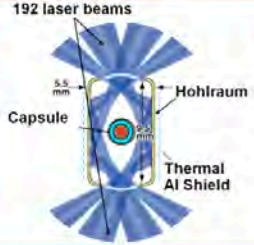

1. Deuterium-tritium fusion creates 14 MeV neutrons
2. Low energy neutrons scatter off the remaining deuterium-tritium and ablator
3. Hohlraum material, mostly gold, is activated and debris is collected
4. Tracer material added to the capsule is activated and collected

To the right is the Diagnostic Insertion Manipulator (DIM) nose cone that position Solid RadioChemistry (SRC) collectors 50 cm from the hohlraum. Two inch diameter ^{nat}V disks (99.75% ^{51}V, 0.25% ^{50}V) were used during these NIF shots. Vanadium metal is frequently used as a SRC collector due to its high melting temperature (1910 °C) and V activation products do not interfere with the gamma detection of the activated gold.

Cross-Section Values From Various Libraries of 14 MeV Neutrons on ^{51}V

	ENDF/B-VI	JENDL-3	JEF-2	CENDL-2	EAF-3	FENDL/A-2	ADL-3T	Average	Std Dev	% Std Dev
^{51}V(n,α)^{48}Sc	14.9 mb	15.6 mb	19.4 mb	15.31 mb	13.94 mb	14.89 mb	15.42 mb	15.57 mb	1.79 mb	11.5 %
^{51}V(n,n-α)^{47}Sc	0.1 mb	0.35 μb	0.19 mb	0.14 μb	2.5 mb	3.84 μb	3.84 μb	0.4 mb	0.93 mb	233 %

^{51}V(n,α)^{48}Sc and ^{51}V(n,n-α)^{47}Sc are two nuclear reactions that occur with ^{nat}V during a NIF shot. As can be seen above there is a large discrepancy in cross section evaluations for ^{51}V(n,n-α)^{47}Sc with 14 MeV nuetrons.[1] After a NIF shot, data from the ^{nat}V collectors can be used to more accurately measure the ^{51}V(n,n-α)^{47}Sc cross section.

Methods

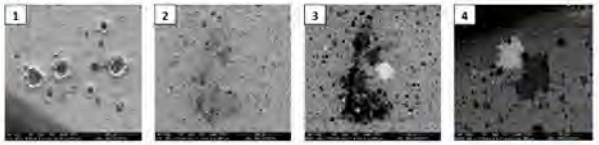

Pictures 1-4 are scanning electron microscope images of a V SRC collector after a NIF shot. The backscattered electron images (3 and 4) show that the collectors are covered in Au and there are spots of Fe (dark) and In (light) hohlraum material.

Picture A shows the V SRC collector after it has been removed from the DIM. To accurately measure the ^{51}V(n,n-α)^{47}Sc cross section, the V disk needs to be dissolved and the Sc has to be separated from the bulk V material.

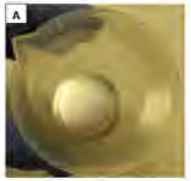

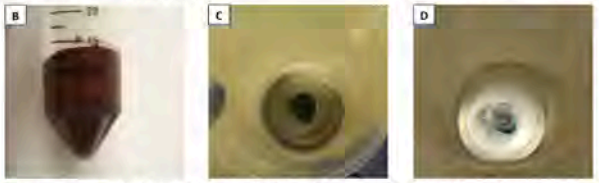

Literature states that V metal dissolves in nitric acid, agua regia, and hot hydrofluoric acid.[2] Many different methods were tested. Passivation occurs (B and C) when using nitric acid or aqua regia to dissolve the V disk. Scandium is detected in the passivation product. Picture D shows V passivation product being dissolved by concentrated hydrofluoric acid. A mixture of both concentrated nitric and hydrofluoric acid completely dissolves the V disk (E and F). Picture G shows Sc being coprecipitated out of solution as ScF_3 using Ce carrier.[3] The yield of this method is <10% which may be due to formation of soluble complex such as ScF^{-4} and/or the Ce carrier not homogenously mixing throughout the solution.

By adding the carrier to the solution while dissolving the V disk in concentrated nitric acid, the Sc does not get trapped in the passivation product and the carrier is homogenously mixed throughout the solution. Fluoride coprecipitation yield, >70%.

Results

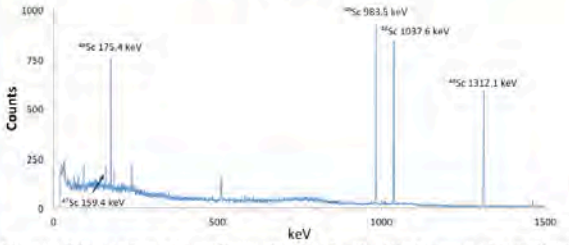

Above is a 3 day spectrum taken at Nuclear Counting Facility of the Sc sample after the V disk was dissolved and Sc was separated from the bulk V material. The precipitate is dissolved using 50/50 (v/v) saturated boric acid and 2 M nitric acid solution. For this sample the ratio of ^{47}Sc/^{46}Sc produced during the NIF shot is 0.0053 ± 0.0006 and the cross section of the ^{51}V(n,n-α)^{47}Sc is calculated* to be 82.8 ± 13.7 μb. A sample from a different shot has a ^{47}Sc/^{46}Sc ratio of 0.007 ± 0.002 and a calculated* ^{51}V(n,n-α)^{47}Sc cross section of 112 ± 33 μb. The two measurements agree within error and have a considerable smaller uncertainty than the evaluated cross section data.[1]

*Assumption made: negligible contribution from ^{50}V(n,α)^{47}Sc and ^{51}V(n,α)^{48}Sc cross section equals 15.57 ± 1.79 mb.[1]

Future Work

The assumption made to simplify the ^{51}V(n,n-α)^{47}Sc cross section calculation may not be correct. Assuming that the cross section of the ^{50}V(n,α)^{47}Sc is the same as ^{51}V(n,α)^{48}Sc reaction, the calculated cross section for ^{51}V(n,n-α)^{47}Sc would decrease by 39 μb. A more accurate way to measure both reaction cross section would be to also analysis an enriched V foil after a NIF irradiate. To the left is a foil holder that can be placed behind a SRC collector during future NIF shots. The foil would also have less bulk material, making sample preparation faster and easier.

Acknowledgement

I would like to thank the Glenn T. Seaborg Institute for giving me this amazing opportunity to spend a summer working at LLNL. Also, I would like to especially thank Evgeny and also Dawn, Ken, Narek, and John for their guidance during this project.

References

1. I.C. Gomes, D.L. Smith and E.T. Cheng, *Status of Cross-Section Data for Gas Production from Vanadium and ^{26}Al from Silicon Carbide in a D-T Fusion Reactor*, 13th Topical Meeting on the Technology of Fusion Energy - 1998 American Nuclear Society Annual Meeting, June 7-11, Nashville, Tennessee (1998)
2. J.L. Brownlee, *The Radiochemistry of Vanadium*, US Atomic Energy Commission Nuclear Science Series NAS-NS 3022 (1960).
3. P.C. Stevenson and W.E. Nervik, *The Radiochemistry of Rare Earths, Scandium, Yttrium, and Actinium*, US Atomic Energy Commission Nuclear Science Series NAS-NS 3020 (1961).

This work performed under the auspices of the U.S. Department of Energy by Lawrence Livermore National Laboratory under Contract DE-AC52-07NA27344.

LLNL-POST-641877

URANIUM ISOTOPIC MEASUREMENTS OF FALLOUT SPHERULES USING ISOTOPE DILUTION MASS SPECTROMETRY

Lucas Boron-Brenner[1], Gary Eppich[2], Kim Knight[2], and Ralf Sudowe[1]

University of Nevada Las Vegas[1], and Lawrence Livermore National Laboratory[2]

Glenn T. Seaborg Institute

UNLV

Goal: To determine uranium concentration and isotopic composition as a function of fallout glass size

1.25 – 2.5 mm Grain Size

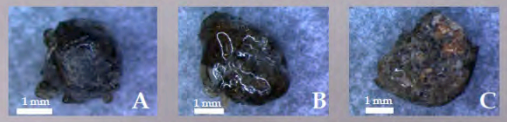

Composed of unmelted environmental soil with a coating of fallout glass.

Soil

Picked clean of fallout glass.

0.6 – 1.25 mm Grain Size

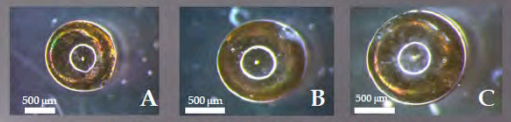

All grains consist entirely of glass; no unmelted soil

0.6 – 1.25 mm Composite

0.3 – 0.6 mm Composite

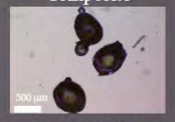

0.21 – 0.3 mm Composite

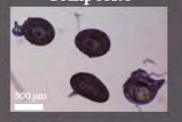

All grains consist entirely of glass; no unmelted soil

INTRODUCTION

Fallout glass, formed during above-ground nuclear tests, primarily consists of materials incorporated from the nearby environment, (e.g. surface soils) as well as fission and activation products, nuclear fuel that did not undergo fission, and non-nuclear components of the device. The detonation causes the fallout glass to become dispersed into the surrounding area, possibly causing the smallest particles to travel farther from ground zero.

Since the beginning of nuclear testing, little focus has been placed on characterization of test fallout. Analysis of this fallout may provide unique insight into the chemistry and physics underlying nuclear weapons detonations. Data obtained through the chemical and isotopic analysis of fallout will likely be essential in a post-detonation nuclear forensics scenario.

In this study, samples containing fallout were collected from a location proximal to ground zero. Soil and fallout particles were sorted by size, and pieces of glassy fallout were physically separated from the soils from which they were collected. Pieces of fallout were dissolved using mineral acids and analyzed by isotope dilution mass spectrometry (IDMS) to determine fallout uranium concentration and isotopic composition.

Sample Preparation
- Soil separation by grain size using a sieve table.
- Picking of fallout glass assisted by optical microscopy.

Chemical Digestion
- Digestion: 2.5 parts HNO_3 to 1 part HF.
- Addition of $HClO_4$ and 3 M HCl producing stock solution.

Sample Spiking
- Addition of ^{233}U spike to aliquots of stock solutions, spike equilibration.

Uranium Separation I
- U-TEVA ion exchange with 4 M HNO_3.
- Column rinsed using 4 M HNO_3, 9 M HCl, and 5 M HCl.
- Uranium eluted using 0.1 M HCl.

Uranium Separation II
- AG1-X8 ion exchange with 9 M HCl.
- Rinsed using 9 M HCl followed by uranium elution using 0.1 M HCl.

Isotopic Analysis
- Analysis performed using MicroMass Isoprobe MC-ICP-MS.

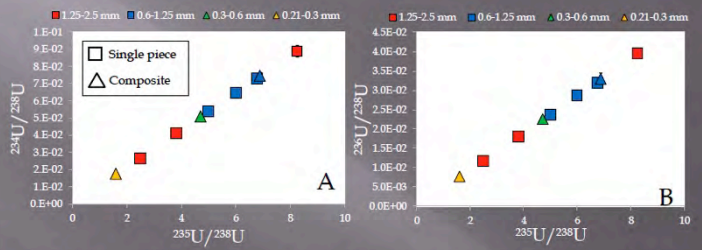

The isotopic composition of individual and composite fallout samples are shown in Panels A and B. These plots demonstrate that the uranium isotopic composition of fallout can be explained through two component mixing between nuclear fuel from the device (approx. 92% ^{235}U) and the natural soil (0.7% ^{235}U). The y-intercept of Panel A represents the $^{234}U/^{238}U$ ratio from the soil end-member. Assuming a device end-member uranium isotopic composition ($^{235}U/^{238}U$ = 92 %), the device $^{234}U/^{235}U$ = 1.09%. When not shown, uncertainty bars are smaller than symbols.

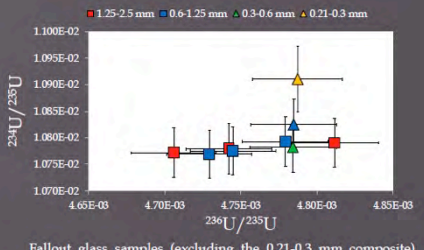

Fallout glass samples (excluding the 0.21-0.3 mm composite) overlap within uncertainty in $^{234}U/^{235}U$ and $^{236}U/^{235}U$, consistent with the two-component mixing model. As in the previous figure, the $^{234}U/^{235}U$ ratio of composite 0.21-0.3 mm is larger. A fraction of glass in the smallest size fraction may have come from a nearby above-ground test, contaminating this size fraction with fallout of a different characteristic $^{234}U/^{235}U$ ratio. The $^{234}U/^{235}U$ and $^{236}U/^{235}U$ ratios measured in these samples may be characteristic of this particular test.

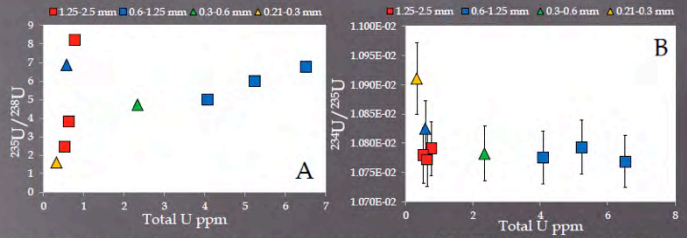

In Panel A, no simple relationship between uranium concentration and $^{235}U/^{238}U$ is observed. The 1.25-2.5 mm samples, which consist of a mixture of unmelted soil and fallout glass, likely vary in U and $^{235}U/^{238}U$ due to their unmelted soil component. The individual 0.6-1.25 mm samples have much higher uranium concentrations than the composite, suggesting that the composites may obscure considerable bead-to-bead heterogeneity in U and $^{235}U/^{238}U$. In Panel B, the 0.21-0.3 mm composite does not overlap within uncertainty relative to most of the other fallout glass samples. This larger ratio suggest an additional uranium component not present in the other size fractions. The source of this additional uranium component may be contamination from another nearby test. Alternatively, the $^{234}U/^{235}U$ ratio may suggest a physical or chemical process occurring during fallout formation not previously identified. When not shown, uncertainty bars are smaller than symbols.

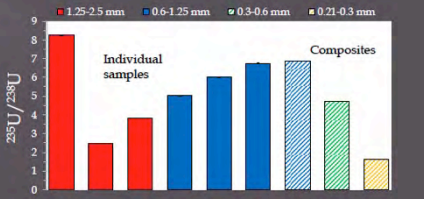

Considerable isotopic variation is observed, both between individual particles, and between particles of different grain sizes. The $^{235}U/^{238}U$ ratio of composite samples decreases with decreasing grain size, suggesting that the smallest fallout glass particles may contain a larger fraction of uranium from soil relative to the device.

This work was performed under the auspices of the U.S. Department of Energy by Lawrence Livermore National Laboratory under Contract DE-AC52-07NA27344. This work was funded by the Laboratory Directed Research and Development Program at LLNL under project tracking code 10-SI-016. LLNL-POST-641637.

Fundamental Study of Scintillating Materials and their PSD Properties

Megan E. Deeds, H. Paul Martinez, Natalia Zaitseva*, Leslie Carman, Andrew Glenn, and Mareena Robinson

Lawrence Livermore National Lab, 7000 East Ave. Livermore, CA 94550

Abstract

Neutron detection is important for the detection of nuclear materials. Scintillation techniques have proven to excel in the detection of neutrons for years. Specifically, organic scintillators show promise due to their ability to detect fast neutrons and more recently, thermal neutrons. Organic scintillators are able to resolve the difference between neutrons and other ionization materials and well as between neutrons types due to pulse shape discrimination (PSD).

There are three types of organic scintillators including crystal, liquid, and plastic. Though crystal and liquid scintillators show greater resolution, they do have their drawbacks. Crystals are fragile and often expensive to grow while liquids pose environmental concerns due to the toxicity of solvents. More recently., "safer" solvents have been explored for liquid scintillators. "Safe" solvents offer higher flash points as well as toxicity. Additionally, plastics have shown promise, as they are durable and relatively inexpensive. One goal of this study is to understand what effects the performance of these materials.

The detection of slow neutrons using organic scintillators is an important area of study. Literature has shown that lithium-6 and boron-10 can achieve thermal neutron detection when added to organic scintillators. This work will show how different lithium compounds effect the PSD capabilities of both liquid and plastic scintillators.

Detection of Neutrons

The ability to detect neutrons depends on the energy levels of the components of the scintillating materials. Electrons within a molecule are excited due to ionization, and after a period of time these electrons relax by releasing energy, usually in the form of light. Typically with these scintillating materials, there are two types of emission, prompt fluorescence and delayed fluorescence. Prompt fluorescence results from an electron excited from the S_0 energy level into the S_1 and relaxing back into the S_0 level (where S is a singlet excited state). Delayed fluorescence requires the interaction of triplet states of pairs of excited molecules. Triplet states are lower energy states which undergo migration within the scintillator material, before they collide producing additional excited singlet states that relax into the singlet ground state with a longer fluorescent lifetime. The difference between the prompt and delayed fluorescence allows for the PSD phenomenon to exist. This process is shown in Figure (a).

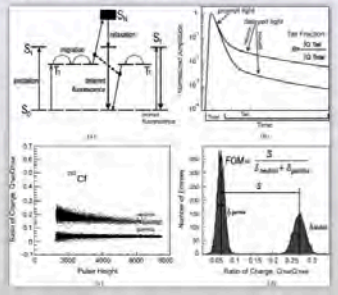

The initial spectrum includes the neutron and gamma waveforms, containing both the prompt and delayed light (b). The pulses with the low fraction of the delayed light result from the excitation produced by gamma interactions, while the pulses with higher proportion of delayed light correspond to the neutron-induced scintillation. By integrating at these different portions of the wave function, a typical PSD diagram is constructed (c). An alternative representation of PSD using figure of merit (FOM) is shown in figure (d). FOM is determined by taking the separation of the peaks of interest and dividing by the sum of full width at half maximum (FWHM) of the corresponding peaks.

Liquid Scintillators

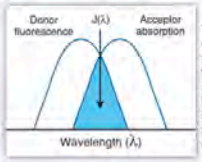

Dyes are used in order to increase the lifetime of fluorescence. This lifetime is the measure of time a photon exists after an excited electron relaxes. As shown in the diagram, once a solvent molecule fluoresces a dye (chosen because the absorption band overlaps with the emission band of the solvent molecule) molecule is available to absorb that light. The dye molecule later emits the photon allowing for the measurement of the fluorescence lifetime. The addition of a secondary dye is favorable because it will likely increase the fluorescence light yield, resulting in greater separation of neutrons and gammas.

Emission spectra of various secondary dyes. Only four of the dyes had PSD and two of those had light yields sufficiently close to DPA.

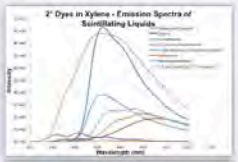

Comparison of FOM of various dyes in a "safe" solvent, PXE (blue)

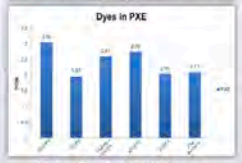

Liquid scintillator under UV light.

Plastic Scintillators

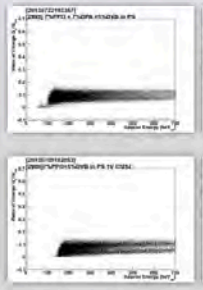

PSD spectra of an investigation of dye composition in plastics. PSD is visible in a blank including PPO. PSD is weakened with the addition of DPA.

Plastic scintillators under UV light.

Future Work

Lithium compounds can be used to further discriminate thermal neutrons from fast neutrons. Currently it is important to determine the compound with the best PSD performance. In order to do so, multiple lithium compounds must be synthesized. Once synthesized, the compounds performance is tested using liquid scintillation. Liquids are quickly and easily made. Once the PSD performance is modeled in the liquid scintillator, the best compounds will be chosen for further study in plastics.

^{6}Li Compound Synthesis

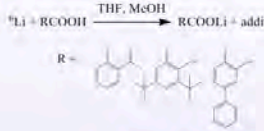

^{6}Li Liquids and Plastics

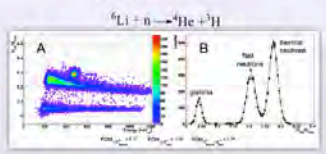

Conclusions

Studying various dyes in p-xylene helped to gain information regarding the effectiveness of secondary dyes. The emission spectra revealed that only four of the eight solvents would be compatible as secondary dyes. This is due to their excitation wavelength being equivalent to that of the emission wavelength of PPO. Of the secondary dyes studied however, none of them proved to have more PSD than DPA.

PXE, a "safe" solvent, shows promise as a liquid scintillator with PSD properties. DPA , a common secondary dye known for great PSD in xylene, does not perform quite as well in PXE. This affect on PSD could be due to the viscosity of the new solvent. Small concentrations of dye is likely creating too much distance between molecules thus, limiting their interaction. This causes less time in the excited state, and less delayed fluorescence.

Dye composition in plastics correlates to the scintillators PSD quality. It is known that higher dye loads increase PSD. This was proven to be true in this study. Additionally, at 1:1 compositions of PPO:DPA, the PSD decreases when compared to the blanks. 2:1 compositions of PPO:DPA result in slightly better PSD.

References

[1] J. B. Birks, The Theory and Practice of Scintillation Counting, Pergamon Press, London, 1964.

[2] N. Zaitseva, A. Glenn, L. Carman, R. Hatarik, S. Hamel, M. Faust, B. Schabes, N. Cherepy, and S. Payne, "Pulse Shape Discrimination in Inorganic and Mixed Single-Crystal Organic Scintillators," *IEEE Transactions on Nuclear Science*, vol. 58, no. 6, pp. 3411-3420, 2011.

[3] N. Zaitseva, B. L. Rupert, I. Pawelczak, A. Glenn, H. P. Martinez, L. Carman, M. Faust, N. Cherepy, and S. Payne, "Plastic scintillators with efficient neutron/gamma pulse shape discrimination," *Nuclear Instruments and Methods in Physics Research A*, vol. 668, pp. 88-93, 2012.

Lawrence Livermore National Laboratory

LLNL-POST-638978

This work was supported by the U.S. DOE, NNSA, Office of Defense Nuclear Nonproliferation, Office of Nonproliferation Research and Development (NA-22)

This work performed under the auspices of the U.S. Department of Energy by Lawrence Livermore National Laboratory under Contract DE-AC52-07NA27344

ENVIRONMENTAL TRANSPORT OF PU: DESORPTION OF PU(IV) IN A MULTI-MINERAL SYSTEM

Chad Durrant[1,2], James Begg[1], Mavrik Zavarin[1], Pihong Zhao[1], Annie B. Kersting[1]

[1]Glenn T. Seaborg Institute, [2]Penn State University

❶ Plutonium Transport

- Globally ~2000 MT Pu released to the environment [1].
- Understanding subsurface Pu transport is of vital importance.
- Mineral colloids identified as an important transport vehicle for Pu.
- Study Pu-mineral colloid interactions to develop transport models.

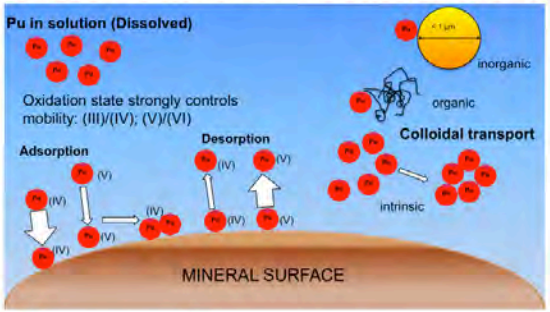

Project Goals

Understanding the behavior of plutonium in complex mineral systems. Specifically, how will adding a second mineral affect the stability of plutonium that is aged onto a first mineral.

❷Experimental Set-up

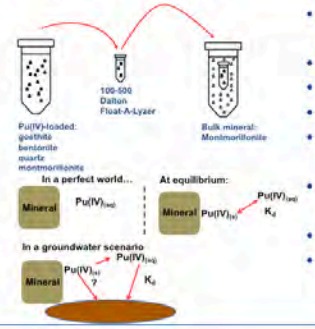

- Studies conducted at pH 4 and pH 8
- Four different minerals
- Aged with Pu(IV)
- [Pu(IV)] is 3 x 10^{-10} M
- 5 mL of aged sample placed in each Float-A-Lyzer
- The bulk mineral montmorillonite
- [mont] is 5 g/L
- Acts as infinite sink to any plutonium that may desorb

❸ Troubleshooting

Initially no plutonium was seen diffusing through the Float-A-Lyzer membrane. To determine the cause of this phenomena two initial possibilities were raised:

- Perhaps the high concentration of montmorillonite was causing interference during liquid scintillation counting
- Perhaps the pore size was not large enough for Pu to diffuse through

Is the pore size large enough for Pu to diffuse through?

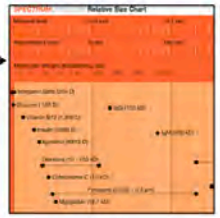

Tested three different sizes of Float-A-Lyzers.

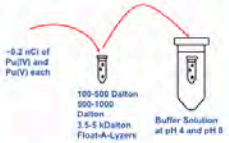

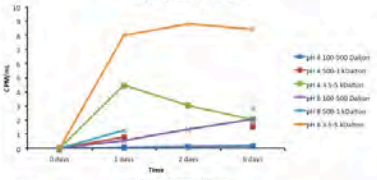

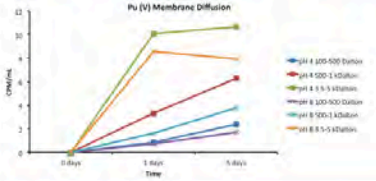

Plutonium does not diffuse through the 100-500 Dalton membrane!

❹ Results

After determining that a larger pore size Float-A-Lyzer was needed the flotation cells were set up again with the remaining goethite and bentonite aged Pu(IV) solutions.

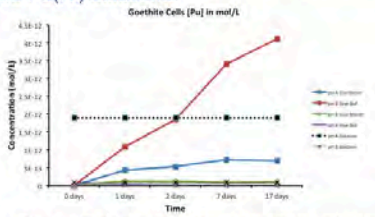

- These two graphs show the ongoing results from the second set of desorption experiments.
- The concentrations represent the amount of plutonium in the bulk phase of the flotation cell.
- The concentration of a 1:1 dilution of the initially free plutonium in the each of the minerals is represented by the dotted line.
- It appears that the addition of a second mineral is increasing the desorption of plutonium from the first mineral in the bentonite cells.

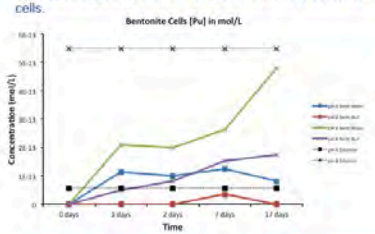

❺ Moving Forwards

Testing the selective affinity for adsorption of plutonium in multiple mineral systems.

Adding organic material to the flotation systems to see the effects on desorption.

❻ Acknowledgements

This work was supported by the Subsurface Biogeochemical Research Program of the U.S. Department of Energy's Office of Biological and Environmental Research. Prepared by LLNL under Contract DE-AC52-07NA27344.

This research was performed under the Nuclear Forensics Graduate Fellowship Program, which is sponsored by the U.S. Department of Homeland Security, Domestic Nuclear Detection Office and the U.S. Department of Defense, Defense Threat Reduction Agency. This material is based upon work supported by the U.S. Department of Homeland Security under Grant Award Number, 2012-DN-130-NF0001-02. The views and conclusions contained in this document are those of the authors and should not be interpreted as necessarily representing the official policies, either expressed or implied, of the U.S. Department of Homeland Security.

1. A. B. Kersting, "Plutonium Transport in the Environment", Inorganic Chemistry, 52 (7), pp. 3533-3546, 2013.

LLNL-POST-

LLNL-POST-761247

Developing Spatially Resolved Analyses of Historical Fallout

Fitzgerald, Marc[1]; Knight, Kim[2]; Stone, Gary[2]; Calderia, Lee[2]; Austin, Kevin[2]; Ramon, Erick[2]; Czerwinski, Ken[1]; Hutcheon, Ian[2]

1. University of Nevada Las Vegas
2. Lawrence Livermore National Laboratory

UNLV Glenn T. Seaborg Institute

Spatially resolved analyses of fallout can guide our understanding of fallout formation

Overview

Nuclear detonations where fireball ground-contact occurs generate significant quantities of nuclear fallout. This material is created by the vaporization, melting, and scouring action of the fireball on the soil immediately surrounding the device. Since fallout incorporates radioactive traces of the device and event, this material is important for nuclear forensics study. The Trinity device, exploded July 16th, 1945, provides a comparatively well-characterized model system for studying fallout-formation. To understand and characterize this material, we conducted analyses using two methods: autoradiography and microscopy. Microscopy techniques included back-scatter (BSE) and energy dispersive x-ray (EDX) scanning electron microscopy (SEM). These techniques complement each other for the purpose of imaging the spatial deposition of the actinide fuel and/or fission products with respect to major element abundances. **Applying combined spatially resolved measurements, we extracted mixing and formation relationships not accessible through bulk dissolution analysis.**

Method

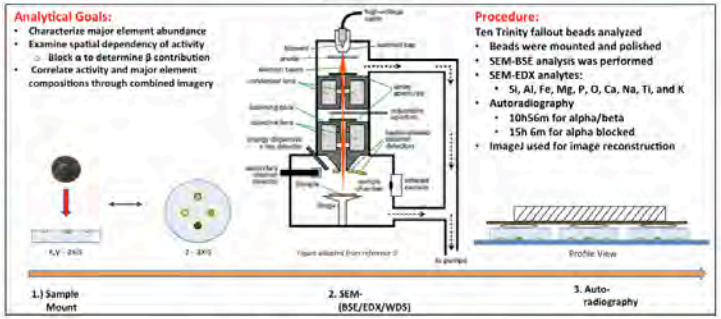

Theory

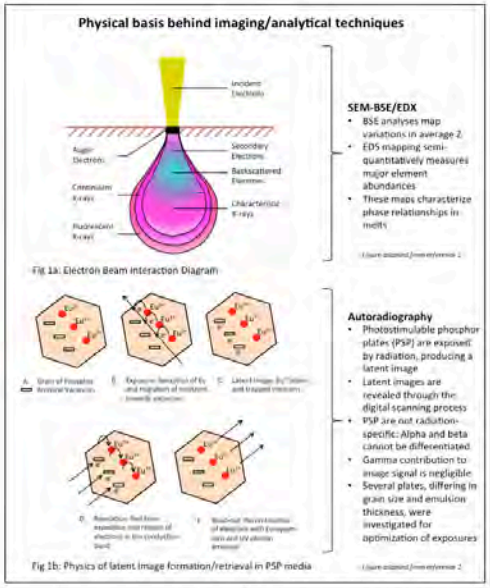

Results and Discussion

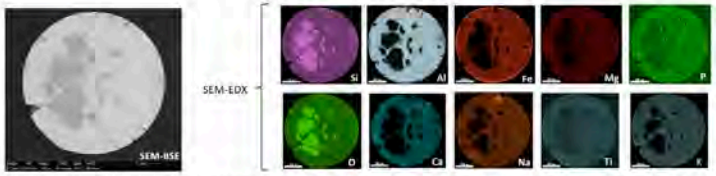

Fig 2: SEM-BSE and EDX of a single representative spherule. For BSE imaging, areas of lighter intensities correspond to higher atomic number. For EDX maps, areas of lighter intensity correspond to elevated elemental abundance in phases. This sample highlights the extensive contrast between silicon-rich inclusions (sample B, below).

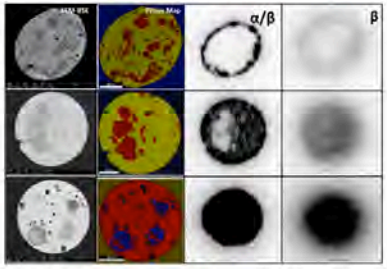

Fig 3: α/β autoradiography shows two distinct modes of spatial activation: surficial and volumetric. The α/β exposure A and C samples demonstrate both extremes (i.e., exclusively surficial or volumetric activation). Exposure B shows some contribution of the two modes. β autoradiography used paper to block α signal to qualitatively confirm that the α/β signal was predominately from α-species (^{239}Pu and ^{241}Am for Trinitite). In most cases, fission products appear to track with alpha species. Despite best efforts, some α-signal had bled through – the basis for this being gamma spectroscopy. Likely beta-emitting isotopes are ^{137}Cs and ^{90}Sr.

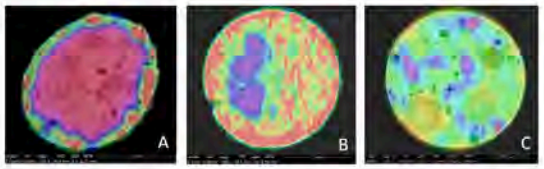

Fig 4: Combined imaging of activity and SEM-BSE analyses reveals the correlation between areas of high activity and high-Z. Warmer colors correspond to areas of higher activity, cooler colors correspond to areas of lower activity. Color scale overlays SEM-BSE images, but is not normalized between spherules.

Examination of corresponding SEM-EDX images (see, for example, Fig 2) show correlations between activity, Ca, Al, Na, K, and Fe. There is an inverse correlation between activity and Si-rich regions. Investigation by EPMA demonstrates that these areas consist of nearly pure silicon dioxide (presumably relict quartz grains), which has a much higher melting point than potassium feldspar (the most likely mineralogical contributor to the CaO-Al_2O_3-SiO_2 rich regions). The preservation of relict quartz would bound maximum heating temperatures of the parent soil to 1700 K. These associations suggest activity dominantly mixed into high abundance, low melting temperature phases. Additionally, activity-iron correlations in most samples suggest iron from the tower tracked the fuel/fission product of the explosion. Alpha and beta activity distributions tend to track one another within samples, contradicting "conventional wisdom" that refractory fuel/fission products are volumetrically distributed and volatile fission products are surficially distributed. (Miller) We hypothesize that observed volumetric and surficial activity distributions are instead a result of solid or partially molten mineral constituents being mixed with molten activity-bearing material. Further investigation and improvements in α/β discrimination is necessary to substantiate this observation.

The Way Forward

Spatially resolved measurements inform formation mechanisms

- Activity–phase correlations would be very difficult or impossible to make using conventional bulk analysis techniques
- We are now developing quantitative high resolution autoradiography to increase the utility of this technique for inter-sample comparisons. See figure 5.
- LA-ICP-MS or SIMS/RIMS based analyses will use the autoradiography information to probe the spatial distribution of actinides and fission products

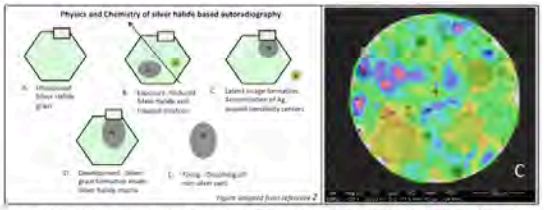

Fig 5: Silver Halide based autoradiography exhibits higher resolution than PSP autoradiography

References

1.) Handbook of Analytical Methods for Materials "Scanning Electron Microscopy"
2.) Laboratory Materials Characterization Facility, Instrumentation
3.) Barth, Nicole "High Resolution Beta Imaging" In Handbook of Radioactivity Analysis. 3rd ed. - Commercially. Michael F. - Ed. Academic: Oxford 2012, pp 1205-1245.
4.) Miller, C. F., A Theory of Fractionation of Fallout from Fossil Surface Nuclear Explosions. 2nd Phase of the Project Technical Report (USNRDL-TR-825, US Naval Radiological Defense Laboratory, 1965

This research was performed under the Nuclear Forensics Graduate Fellowship Program, which is sponsored by the U.S. Department of Homeland Security, Domestic Nuclear Detection Office. This work was also performed under the auspices of the U.S. Department of Energy by Lawrence Livermore National Laboratory under Contract DE-AC52-07NA27344. LLNL-POST-XXXXXX

LLNL-POST-760588

Characterization of TBP using FTIR-ATR and Carbon Stable Isotopes

April R. Gillens[1], Michael Singleton[2], and Brian A. Powell[1]; [1]Environmental Engineering and Earth Sciences, Clemson University, Clemson, SC
[2]Environmental Radiochemistry Group, Chemical Sciences Division, Physical and Life Sciences Directorate, Lawrence Livermore National Laboratory, Livermore, CA

Research Objectives

The objective of this research is to determine the carbon stable isotope signatures of tributyl phosphate (TBP) and its degradation products after contact with nitric acid and sodium hydroxide for the purpose of identifying if there is a unique carbon isotope signature in nuclear reprocessing and solvent disposal. The degradation products considered in this research are limited to dibutyl phosphate (DBP) and butanol. In order to meet this objective, studies will be conducted involving the following instrumentation:

- Fourier Transform Infrared Spectroscopy with Attenuated Total Reflectance (FTIR-ATR)
- Gas chromatography Flame Ionization Detection (GC-FID)
- Gas Chromatography Combustion Isotope Ratio Mass Spectrometry (GC-C-IRMS)

TBP Degradation Mechanisms

Acidic Hydrolysis vs. Basic Hydrolysis

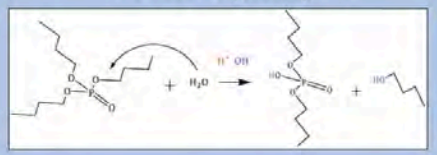

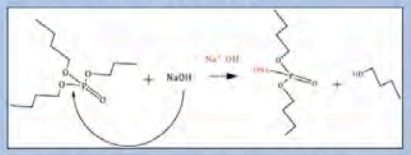

$$(C_4H_9O)_3PO + H_2O \xrightarrow{H^+ + OH^-} (C_4H_9O)_2PO(OH) + C_4H_9OH$$

$$NaOH + CH_3 - CH_2 - CH_2 - CH_2 - O\cdots PO(OC_4H_9)_2 \xrightarrow{OH^- + Na^+} NaO - P - O(OC_4H_9)_2 + C_4H_9OH$$

Carbon isotope analysis should confirm the degradation mechanisms of TBP in acidic and alkaline conditions. A carbon isotope fractionation is not expected for TBP in alkaline conditions because the P—O bond would rupture keeping the carbon in the molecule intact. A carbon isotope fractionation is expected for TBP in acidic conditions because of the cleavage of the C—O bond associated with TBP degradation under this condition. Hence, this work will determine whether there is a unique carbon isotope signature for TBP in nuclear reprocessing and disposal by studying the fundamental characteristics of TBP in acidic and basic hydrolysis. The reaction mechanisms for TBP degradation in acidic and alkaline hydrolysis are distinct. Although the two mechanisms proceed differently, the same degradation products are generated in addition to other products specific to the compound used to degrade the TBP molecule. The majority of degradation products resulting from acidic hydrolysis can be found in both aqueous and organic phases while most of the degradation products from alkaline hydrolysis are found in the aqueous phase. The difference in how TBP degrades in acidic and alkaline media could have major implications on the "signature" of the molecule as a result of its use in nuclear reprocessing and solvent disposal.

FTIR-ATR Peak Intensity Ratio Technique

Acidic Hydrolysis vs. Basic Hydrolysis

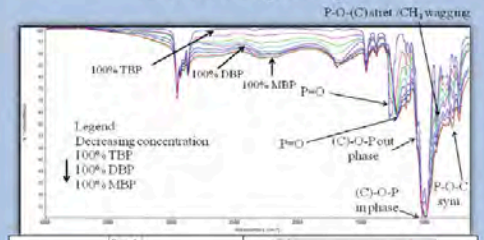

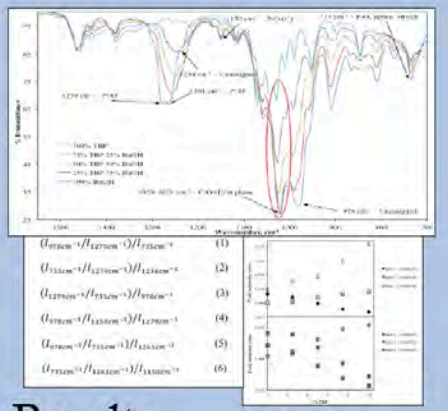

FTIR-ATR Results

A. A sample of TBP degraded in 8 M HNO_3 was evaluated using the peak intensity ratios above. The linear regression developed for a TBP/DBP system saturated in 8 M HNO_3 was used. Ratios 1 and 2 are more reliable and the results of ratio 3 do not reflect the conditions of the sample. After five weeks of hydrolysis, an average of 68% of DBP is produced according to ratios 1 and 2. These results have not be verified by gas chromatography. **B.** This figure describes the average amounts of TBP remaining and butanol formed along with their associated uncertainties for a TBP alkaline hydrolysis experiment involving 12.5 M NaOH, which was characterized by the FTIR-ATR technique using a saturated and unsaturated TBP/butanol system and gas chromatography.

A.

Table 4 Reevaluation of peak intensity ratios of TBP with 8 M HNO_3

Time	Ratio 1	% DBP	Ratio 2	% DBP
4	0.0121	9.74	0.00785	12.30
12	0.0122	11.24	0.00797	13.81
24	0.0130	20.47	0.00856	21.05
30	0.0131	21.97	0.00866	22.15
36	0.0132	23.27	0.00879	23.76
48	0.0138	29.71	0.00908	27.35
840	0.0167	62.59	0.01237	73.42

B.

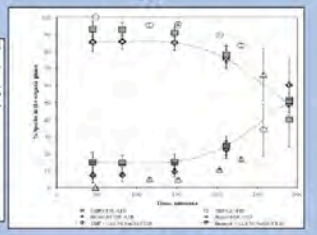

Carbon stable isotope signatures of TBP

The GC-C-IRMS system consists of an Agilent 6890 gas chromatograph coupled with a combustion furnace, which leads to an IsoPrime isotope ratio mass spectrometer. The Agilent 6890 gas chromatograph is equipped with a 30 meter by 0.25 millimeter (inner diameter) HP-5MS (5% Phenyl Methyl Siloxane) Ultra Inert fused silica capillary column with 0.25 µm film thickness. Samples are introduced using a splitless/purge injection port set at 250°C. The GC oven is heated using the following program: isothermal for 1 minute at 50°C, 8°C/min to 100°C, 16°C/min to 230°C, 100°C/min to 300°C, and isothermal for 2 minutes for a runtime of 18.08 minutes. Helium is used as carrier gas through the column with a constant flow rate of 0.8 mL/min and average velocity of 32 cm/sec.

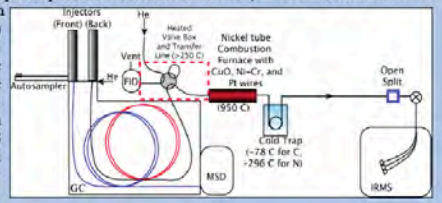

Acknowledgements

This material is based upon work supported by the U.S. Department of Homeland Security under Grant Award Number, 2012-DN-130-NF0001-02. The views and conclusions contained in this document are those of the authors and should not be interpreted as necessarily representing the official policies, either expressed or implied, of the U.S. Department of Homeland Security. This work performed under the auspices of the U.S. Department of Energy by Lawrence Livermore National Laboratory under Contract DE-AC52-07NA27344.

References

[1]W. W. Schulz and J. D. Navratil, The Science and Technology of Tributyl Phosphate, Vol. 1 CRC Press, Boca Raton, FL (1984).
[2]A. R. Gillens and B.A. Powell, *Journal of Radioanalytical and Nuclear Chemistry* Vol. 296 No. 2 (2013) 859–868 DOI 10.1007/s10967-012-2147-6

LLNL-POST-637732

Bonding and Redox Behavior in Actinide Coordination Complexes: A First Principle Study

Mitchell Goshert,[1] Patrick Huang,[2] and Justin Walensky[1]
Physical and Life Sciences Directorate and Glenn T. Seaborg Institute
[1]University of Missouri, Columbia
[2]Lawrence Livermore National Laboratory

INTRODUCTION – REDOX POTENTIAL

- Aqueous uranyl and plutonyl dinitrates are common by-products of nuclear fuel reprocessing.
- What is their long-term mobility and fate?
- Oxidation state determines solubility and consequently the mobility in the environment.
- What are the thermodynamic parameters characterizing the transformation between oxidation states?
- Actinides in solution exhibit a large variation in oxidation state and coordination number.
- Contributions due to variations in actinide speciation difficult to disentangle experimentally.
- Calculations of reduction potential can provide useful insight on the energy required to reduce these actinide species.

THEORETICAL METHODOLOGY

Hartree-Fock (HF)

$$\left[-\frac{\hbar^2}{2m}\nabla_i^2 + V_i^{\text{eff}}(\mathbf{r}_i)\right]\psi_i(\mathbf{r}_i) = \varepsilon_i\psi_i(\mathbf{r}_i)$$

- Mean field approximation: Each electron feels the same averaged, effective potential due to the remaining electrons.
- Does not include electron-electron correlation → qualitative, but not quantitatively accurate.
- Useful as starting point for higher-level theories.

Density Functional Theory (DFT)

- Mean-field theory (like Hartree-Fock)
- Approximate inclusion of electron correlation via model exchange-correlation functional v_{xc}.
- We employ the B3LYP approximation for v_{xc}:
  1. Generally improves bond energies and lengths over HF.
  2. Better-suited for localized d- or f-electrons (minimizes self-interaction error).

SOLVENT MODEL

Conductor-like Polarizable Continuum Model (CPCM)

- Solvent effects are an important influence on reduction potentials.
- Model solvent as a continuum dielectric.
- Need to assume a conductor-like cavity containing solute.
- CPCM well-established for polar solvents (e.g., water).

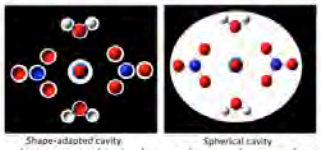

- For large, unspherical complexes, shape-adapted cavities are necessary.

CALCULATION OF REDUCTION POTENTIALS

- Free energies are calculated relative to a standard hydrogen electrode.

$$\mathrm{An^{VI}} + e^- \rightarrow \mathrm{An^{V}}$$
$$\tfrac{1}{2}\mathrm{H_2} + \mathrm{H_2O} \rightarrow \mathrm{H_3O^+} + e^-$$
$$\mathrm{An^{VI}} + \tfrac{1}{2}\mathrm{H_2} + \mathrm{H_2O} \rightarrow \mathrm{An^{V}} + \mathrm{H_3O^+}$$

OPTIMIZATION OF BOTH U(VI) AND U(V) SPECIES

- The structures of the $UO_2(NO_3)_2(H_2O)_2$ complex in both U(VI) and U(V) oxidation states were optimized.
- Vibrational analysis was employed to verify the stability of optimized structures.

- The optimized structures of U(VI) (left) and U(V) (right).

STRUCTURES

$U^{VI}O_2(NO_3)_2(H_2O)_2$ – Bond Lengths

	HF (gas)	HF (solv)	B3LYP (gas)	B3LYP (solv)	Expt.
U=O [Å]	1.71	1.71	1.77	1.77	1.76
$U\text{-}O_{H2O}$ [Å]	2.56	2.53	2.55	2.52	2.45
$U\text{-}O_{NO3}$ [Å]	2.50	2.53	2.49	2.50	2.48

*Experimental data from Dalley, N.K.; Mueller, M.H.; Simonsen, S.H. *Inorg. Chem.* **1971**, *10*, 323.

- B3LYP shows an improved U=O bond length over HF to within ~ 0.01 Å.
- Both HF and B3LYP yield significant lengthening of both $U\text{-}O_{H2O}$ bonds relative to experiment.
- Both HF and B3LYP accurately predict the $U\text{-}O_{NO3}$ bond length within ~0.02 Å.

$U^{V}O_2(NO_3)_2(H_2O)_2$ – Bond Lengths

	HF (gas)	HF (solv)	B3LYP (gas)	B3LYP (solv)	Expt.
U=O [Å]	1.80	1.81	1.84	1.85	-
$U\text{-}O_{H2O}$ [Å]	2.73	2.63	2.71	2.62	-
$U\text{-}O_{NO3}$ [Å]	2.67	2.63	2.61	2.61	-

- Uranyl V bond lengths show ~0.1 Å increase on average over uranyl VI.

REDUCTION POTENTIALS

	E^0 (gas) HF	E^0 (solv) HF	E^0 (gas) DFT	E^0 (solv) DFT
$U(VI) + e^- \rightarrow U(V)$	2.12	4.22	2.86	4.60
$½H_2 + H_2O \rightarrow H_3O^+ + e^-$	-8.02	-4.67	-8.96	-5.78
Reduction Potentials	-5.90	-0.45	-6.10	-1.18

- Inclusion of solvation effects yields a ~ 4.9 eV improvement over the gas phase model.
- Discrepancy between E^0 (solv) and expt. likely due to:
  1. Errors in H_2 half-reaction.
  2. Lack of explicit second coordination sphere.
- Errors for calculated actinide reduction potential typically ~ 2-3 eV
  (Hay, J. P.; Martin, R. L.; Schreckenbach, G. *J. Phys. Chem. A* **2000**, 104)
- Experimental data for the reduction potential of $UO_2(H_2O)_5$ is 0.16 eV, meaning our data is reasonable
  (Brand, J. R.; Cobble, J. W. *Inorg. Chem.* **1970**, *9*, 912.)

CONCLUSIONS – REDOX POTENTIALS

- Benchmark studies have been done on $UO_2(NO_3)_2(H_2O)_2$ VI and V
- Our model involves an explicit representation of the first coordination sphere plus a continuum dielectric for the solvent environment.
- Solvation effects are essential for description of red. potentials.

INTRODUCTION – BONDING BEHAVIOR

- Uranium trioxide, UO_3, is the major precursor used for nuclear energy throughout the world.
- However, due to its poor solubility in organic solvents, little chemical information is known about UO_3.
- Examining the structure, bonding, and reactivity of analogs will provide insight into UO_3 chemistry.
- The Bart group at Purdue University has synthesized two tris(imido)uranium complexes which are isoelectronic with UO_3.
- *Ab Initio* methods were used to calculate the ground state structure of the synthesized compounds.

STRUCTURES – GEOMETRY OPTIMIZATION

- Geometry optimizations were performed on both the $U(PDI)(NDIPP)_3$ (left) and $U(PDI)(NMes)_3$ (right)

		Exp.	Comp.	Exp.	Comp.
$U\text{-}N_{PDI(left)}$	[Å]	2.609	2.621	2.552	2.581
$U\text{-}N_{PDI(center)}$	[Å]	2.587	2.584	2.580	2.566
$U\text{-}N_{PDI(right)}$	[Å]	2.609	2.641	2.553	2.578
$U\text{-}N_{imido(axial)}$	[Å]	1.966	2.014	1.995	2.009
$U\text{-}N_{imido(eq.)}$	[Å]	2.021	2.032	2.024	2.030
$U\text{-}N_{imido(axial)}$	[Å]	1.965	2.017	1.992	2.010

CONCLUSIONS – BONDING BEHAVIOR

- A successful geometry optimization has been completed on the $U(PDI)(NDIPP)_3$ complex with bond lengths within ~0.05 Å accuracy
- The $U(PDI)(NMes)_3$ optimization has not fully converged but demonstrates an accuracy within ~0.03 Å.

ACKNOWLEDGEMENTS

- M.G. gratefully thanks the Glenn T. Seaborg Institute and Laboratory Directed Research and Development for their financial support.

This work performed under the auspices of the U.S. Department of Energy by Lawrence Livermore National Laboratory under Contract DE-AC52-07NA27344.

LLNL-POST-641750

Tritium and Stable Isotope Survey of California Surface Water

Patrick A. Harms[1], Jean E. Moran[1], Ate Visser[2], Brad K. Esser[2]
[1]California State University, East Bay, Department of Earth and Environmental Sciences
[2]Chemical Sciences Division, Glenn T. Seaborg Institute, Lawrence Livermore National Laboratory

Abstract

The purpose of this study is to characterize the isotopic signature of precipitation in California watersheds. Measurements of tritium, ^{2}H and ^{18}O from surface water are used as a proxy to identify regional isotopic features.

Introduction

Tritium (^{3}H) and the stable isotopes of water (^{2}H and ^{18}O) are used to examine watershed dynamics, identify water provenance and determine water residence times. These isotopes are extremely useful as a natural tracer because they follow the path of water as part of the water molecule. Stable isotopes in precipitation have a strong spatial signal that indicates the source of the water. Tritium, which is produced cosmogenically in the upper atmosphere, has a strong temporal signal that allows for age dating of water. Large quantities of ^{3}H were created by atmospheric thermonuclear weapon testing between 1953-1963. Current tritium concentrations in precipitation are approaching pre-nuclear levels.

The strong topographic gradient in California (Pacific Ocean to Sierra Nevada) results in distinct tritium and stable isotope signatures, making these tracers especially useful in water resources and age dating investigations.

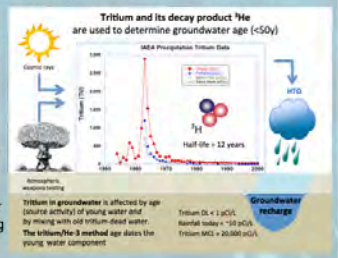

Methods

Field

- Over 40 surface water locations visited across California
- Tritium (^{3}H) and stable isotope (^{2}H and ^{18}O) samples collected in non-preserved 1L and 30 ml glass bottles respectively.
- Water quality parameters recorded with YSI 556.

Lab

Tritium measurements by ^{3}He accumulation (LLNL)

- ^{3}H samples degassed under vacuum to remove decay-product ^{3}He. ^{3}He accumulated for at least 21 days.
- ^{3}He cryogenically separated and measured by mass spectrometry.

Stable Isotopes (CSUEB)

- ^{2}H and ^{18}O measured by cavity ring-down laser absorption spectrometer.

In the field, sampling and recording water quality parameters.

Samples hanging on manifold for degassing under vacuum.

Samples kept frozen with dry ice after cryogenic separation of ^{3}He gas from water.

Results

Stable Isotopes

- **δD and $\delta^{18}O$** are expressed as $\delta(\text{in permil}) = [(R_{sample}/R_{standard})-1]*1000$, where R is ratio of heavy to light isotopes.
- **The Global Meteoric Water Line (GMWL)** represents empirical relationship between δD and $\delta^{18}O$ found in meteoric water.
- **Pacific Ocean** sample (blue circle) is similar **to Vienna Standard Mean Ocean Water** (VSMOW: $\delta D=0$ and $\delta^{18}O=0$).
- **Elkhorn Slough** (also in blue circle) is similar to Pacific due to **ocean influence.**
- **Estuary** samples (red circle) show **evaporation effects**: heavier (less negative) $\delta^{18}O$ and δD than source water (Pacific Ocean). This effect is stronger for hydrogen than oxygen.
- **Coastal samples** are **lighter** than ocean water due to preferential evaporation of light isotopes.
- **Salinas River** sample (green circle) also shows **evaporation effects** with coastal water as source.
- **Inland samples** are **lighter** than coastal samples due to rainout of heavy isotopes.
- **Lagunitas Creek** (purple circle) and some inland samples show **deuterium excess** from re-evaporation and precipitation of terrestrial water.

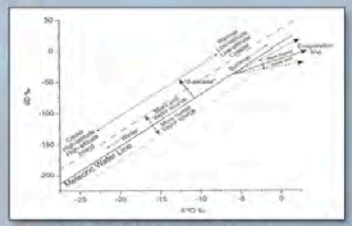

GMWL and factors that affect isotopic ratios of deuterium and oxygen (McGuire and McDonnell, 2006).

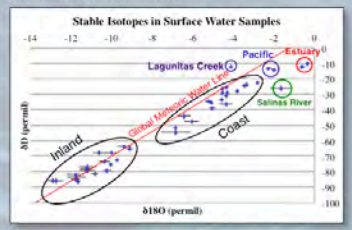

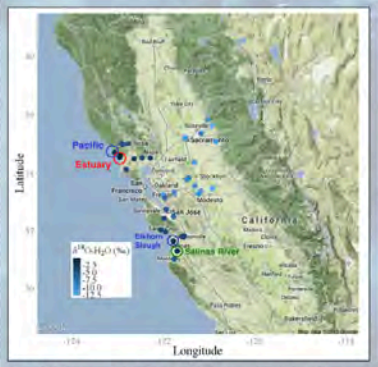

Map of $\delta^{18}O$ in sampled surface water. Strong west to east gradient visible due to rainout of heavier isotopes near coast.

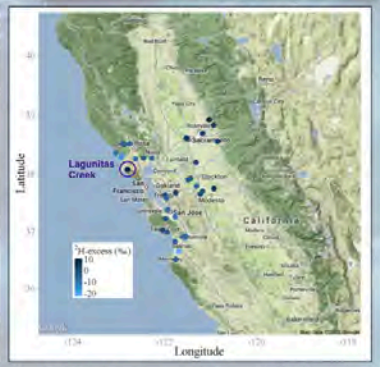

Map of surface water samples with deuterium excess. Most d-excess occurs inland, with the exception of Lagunitas Creek.

Tritium

- **High** concentration of tritium found in **Alameda Creek** and **San Benito River** (red bars).
- Tritium concentration generally **higher** with **less variability** at **high elevation** rivers (green bars).
- Tritium concentration **significantly lower below Folsom Lake** (striped bar), showing effects of reservoir on tritium decay.

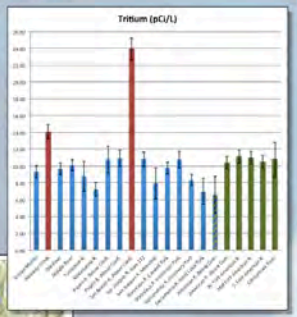

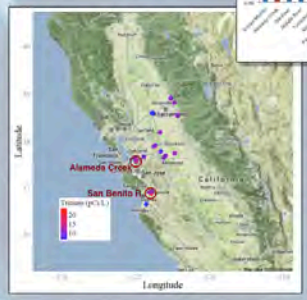

Discussion and Future Work

Discussion

- Preliminary tritium data shows possible elevation gradient and reservoir effects.
- Stable isotope results are consistent with the known coastal to inland and low to high elevation gradients
- Evaporation effects are also apparent from δD and $\delta^{18}O$ offset from the GMWL.

Future Work

- **Spring sampling** - Surface waters will be resampled during the spring runoff period when precipitation signal will be stronger.
- **More watersheds** - Future sampling will include watersheds farther to the north and south as well as the Sierras.
- **Continue tritium analysis** – Because of 21 day accumulation period, not all samples were analyzed in time to be included with these results.

This work performed under the auspices of the U.S. Department of Energy by Lawrence Livermore National Laboratory under Contract DE-AC52-07NA27344.

LLNL-POST-641739

High-Energy Neutron Foil Activation for Davis Cals

Corey Keith[1], Bryan Bandong[2], Robert Haslett[2], Kip Harward[2], Tzu Wang[2], Kevin Roberts[2]

[1]Texas A&M University, Department of Nuclear Engineering, College Station, TX

[2]Lawrence Livermore National Laboratory, Physical and Life Sciences, Chemical Sciences Division, Livermore CA

Davis Cals are inter-laboratory measurements and calibration comparisons of "threshold detector products". High-energy neutron foil activation is used for the isotope production, and the goal is to model this process and compare to experimental results.

Introduction

Radioanalytical measurements on activation species are being performed by LLNL, LANL, and PNNL. The activation species used for the inter-laboratory measurements are produced at the 76-inch Cyclotron at UC Davis Crocker Nuclear Laboratory by irradiating various detector metal foils with high-energy neutrons produced from bombarding a thick beryllium target with 40 MeV deuterons. The existing nuclear data for (d,n) reactions for beryllium, as well as production cross sections for the foils, are very limited in the evaluated energy ranges of the fast neutron spectrum. As a result, it was proposed to use physics models and Monte Carlo codes to simulate isotope production and compare with recent experimental results.

Neutron Flux Profile on Au Foil

To evaluate the differences between physics models and beam width on isotope production, the neutron flux profile on Au foil was evaluated.

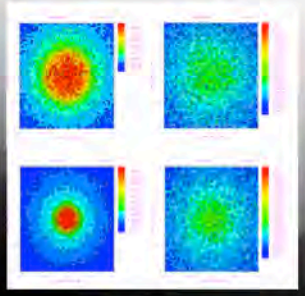

Top Left: INCL4 0.5 cm beam width; Bottom Left: INCL4 0.25 cm beam width; Top Right: Bertini 0.5 cm beam width; Bottom Right: Bertini 0.25 cm beam width

Setup

Various physics models that use both intranuclear cascade (INC) and evaporation physics were used to model (d,n) reactions. Early results showed that, for 40-MeV deuterons, changes in evaporation models had little impact, and so differences between three INC models (CEM03[1], Bertini[2] and INCL4[3]) were evaluated. MCNPX 2.7 was used to evaluate neutron transport in the system and reaction rates in the foils.

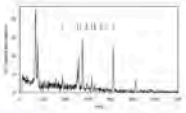

Top: Picture of Beryllium Target and foil assembly Bottom: MCNP modeled geometry Right: Gold foil Gamma Spectrum[4]

Isotope Production

Isotope Production for the gold and titanium foils were evaluated using MCNPX and the ENDF and TENDL cross sections. The activation run was conducted on 12/27/2012

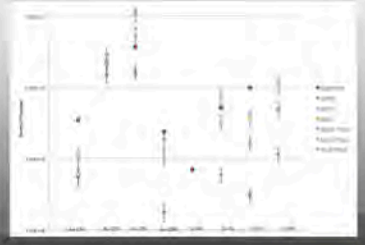

Neutron Flux

Neutron Flux for various INC physics models evaluated for a for a 6.0 ± 1.7 μA beam current.

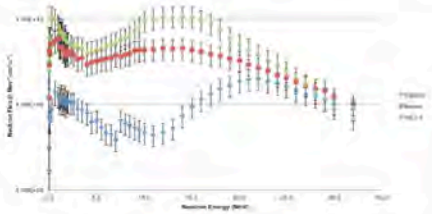

Discussion

The three INC models all have limits of reliability in the energy range being explored when compared with recent experimental data. The TENDL cross sections for higher energy are in good agreement for the ^{195}Au, ^{196}Au, ^{46}Sc, ^{48}Sc residual cross sections. Further work is needed to asses production pathways and cross sections for ^{44}Sc, ^{47}Sc, and ^{194}Au.

References:

1. S.G. Mashnik, et al., LANL Report LA-UR-05-7321, Los Alamos, 2005, RSICC Code Package PSR-532,
2. H.W. Bertini Phys. Rev., 131 (1963), p. 1801
3. A. Boudard *et al*, Phys. Rev. C, 66 (2002), p. 044615
4. J. J. Wilkens, Activation of Implanted Gold 88 Proton Beams, NPTC (2004) 93

This work performed under the auspices of the U.S. Department of Energy by Lawrence Livermore National Laboratory under Contract DE-AC52-07NA27344.

IM: 761065 Release: LLNL-POST-641742

NUCLEAR ENGINEERING
TEXAS A&M UNIVERSITY

Validation of a Phenomenological Fission Model

Morgan Kelley[1], Walid Younes[2], Jennifer Jo Ressler[2]

[1]Washington State University, Department of Chemistry, Pullman, WA

[2]Lawrence Livermore National Laboratory, Physical and Life Sciences, Nuclear Physics Division, Livermore CA

Fission data are very useful for both forensic and basic science applications. Unfortunately, these data often cannot be easily measured experimentally. Therefore, fission models/theories play an important role to fill in the gaps left by experiment. We will determine the extent to which the fission model GEF can be trusted.

GEF: GEneral Fission model

GEF[1] uses Monte Carlo methods used to calculate:

- Element & isotope yield distribution, before and after neutron emission
- Mass chain yields
- Isomer yields
- Angular momentum distribution
- Prompt gamma and neutron spectra
- Total kinetic energy of fragments
- Numerous other fission observables

Uncertainties are determined based on perturbed parameters during iterative calculations.

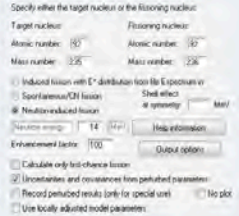

First Assessment: GEF vs. Experiment

Due to larger experimental uncertainties, the Pu239 Thermal data and GEF data match fairly well, while the U235 Thermal data from experiment is often outside of the GEF values.

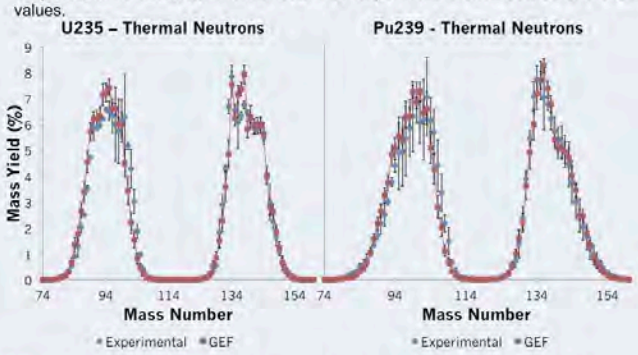

To treat the data in a more rigorous way, χ^2 for each fission product mass was calculated for various nuclides, and compared to the asymmetry:

$$Asymmetry = (Mass(Fragment) - 1/2\ Mass(Nuclide))^2 / Mass(Fragment)^2$$

$$\chi^2 = [Yield(Exp) - Yield(GEF)]^2 / Uncertainty(Exp)^2$$

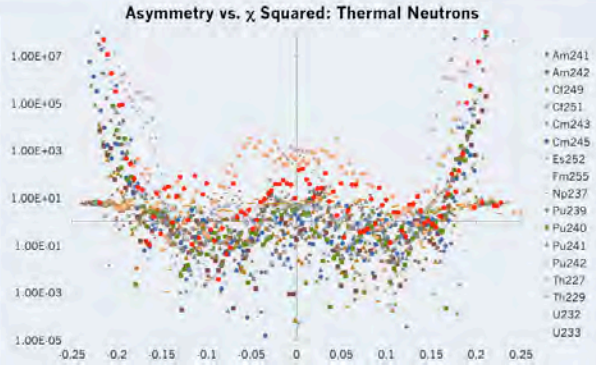

A single χ^2 value was then calculated for each nuclide and compared to the 95% critical value, testing if an obvious reason to reject the model existed. For low-yield masses, GEF's calculated yields are eclipsed by their uncertainties. To exclude these values from the χ^2 calculation, a yield threshold was set and systematically tested. These χ^2 values were calculated taking correlation into account:

$$\chi^2 = \Delta Y^T \times V^{-1} \times \Delta Y$$

ΔY is a vector containing the difference between experimental and GEF yields for each mass, and V is the covariance matrix of the calculated GEF yields.

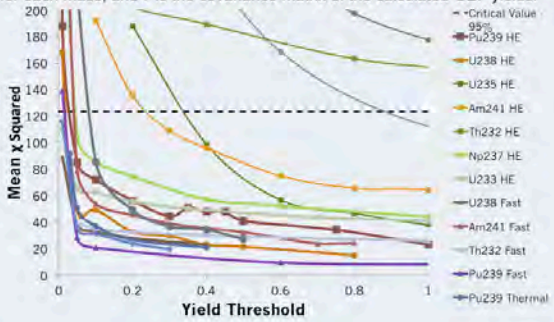

Mass-Chain Yields

In most cases, GEF does an acceptable job of reproducing experimental yields. However, for particular nuclides, the GEF calculations match experimental data mostly thanks to the large uncertainties that GEF calculates.

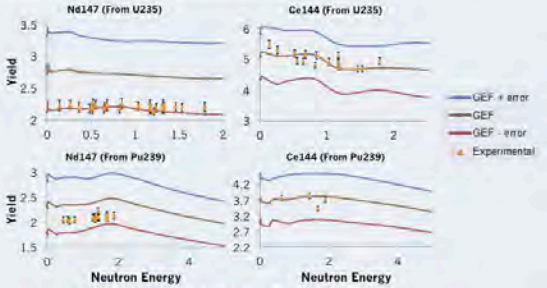

Uncertainty Analysis

χ^2 values for most nuclides are well below the 95% confidence limit (GEF may be overestimating uncertainties). Edited the GEF code to include an error factor: a factor by which the internal GEF parameters – the parameters perturbed to generate the calculated uncertainty – are multiplied by. Investigated the effects of varying the error factor. Attempted to decrease the uncertainty without causing χ^2 to increase to the 95% critical value. In all cases except U235 thermal, the uncertainty calculated by GEF can be reduced.

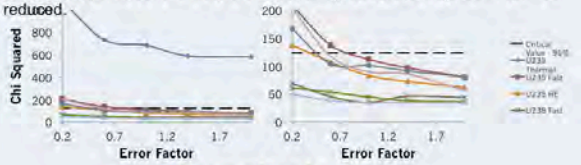

Conclusions

1. For many nuclides, GEF does an acceptable job of reproducing experimental values within experimental error.
2. GEF gives a good starting point for an estimate of experimental yields. However, the type of validation presented here is critical to properly use these estimates and their respective uncertainties.
3. As a phenomenological model, GEF is useful to more fundamental approaches because it helps us understand many important features of fission.

1. K.-H. Schmidt and B. Jurado, JEF/DOC 1423 (2011). GEF code and documentation available for download at http://www.cenbg.in2p3.fr/-GEF-

Prepared by LLNL under Contract DE-AC52-07NA27344. LLNL-POST-641741

Development of a Chemical System for Rutherfordium

Jeff Rolfes[1], John Despotopulos[1,2], Roger Henderson[2], Ralf Sudowe[1]
[1]University of Nevada, Las Vegas
[2]Lawrence Livermore National Laboratory

Background

Studies of the chemical properties of the heaviest elements have always been difficult due to the short half-lives and low cross sections involved. To solve this problem, atom-at-a-time methods are used to determine the properties of short-lived isotopes. Extremely fast kinetics for the chemical reactions studied (on the same order as the nuclide's half-life) are required and the system should have potential for automation. One potential technique, extraction chromatography, offers a way of investigating rutherfordium's properties, without the solvent waste generated in liquid-liquid extractions.

A fast systematic method involving the use of a ligand with higher inner group selectivity is necessary to discover more about element 104. Using the homologs, zirconium and hafnium, studies can be performed using liquid-liquid extractions and extraction chromatography. From literature reviews, thiacrown ethers, tertiary amines, and calixarenes show promise in extracting group 4 elements. The development of an extraction system for rutherfordium based on these extractants can further elaborate on its properties.

40 Zr

72 Hf

104 Rf

Purpose

While the primary goal of research involving rutherfordium and its homologs is to study superheavy element chemistry, this research and techniques can be directly applied to zirconium separations in post-detonation material as zirconium is a major fission product. The speed of separations required for superheavy element chemistry is on the order of seconds. SCUREF's *Technical Mission Area 1* specially mentions speed accuracy and precision concerning the analysis of nuclear materials.

The surrounding ligands will be all tested, beginning with TEHA. All of them have shown promise in the extraction of zirconium and hafnium in literature, but have not been fully examined for their usefulness in fast chemistry.

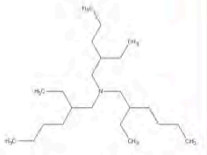

Tris-2-ethylhexyl amine (TEHA)

Dicyclohexano-18-crown-6

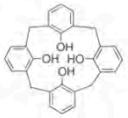

Calix[4]arene

Calix[6]arene

Thiahexa-18-crown-6

Procedure

To initially examine the ligand for its suitability for superheavy element chemistry, a solvent extraction is first performed on the suspected homologs of the element of interest. An aqueous phase of varying acid concentrations is prepared and added to an organic phase with the dissolved ligand.

A spike of a radioactive tracer (either ^{89}Zr, ^{95}Zr, or ^{175}Hf) is then added to the phases.

The spiked phases then are mixed vigorously on a shaker for 30 minutes.

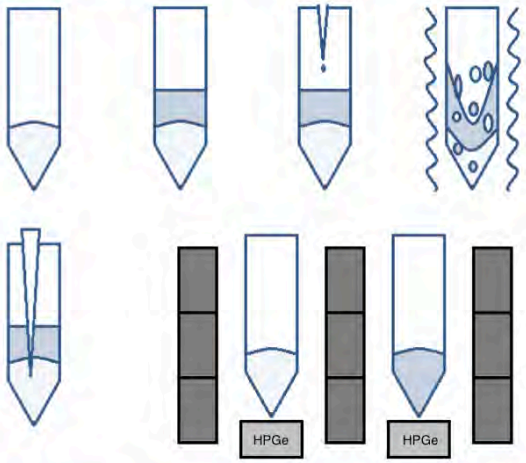

After equilibrium has been reached, the aqueous and organic phases are separated into different vials.

The phases are currently counted on a HPGe detector due to the interference of the ^{95}Nb peak being 10 keV away from the ^{95}Zr peak. In the future, samples will be counted on an automated NaI detector using a ^{89}Zr tracer.

Physical and Life Sciences Directorate

Preliminary Results

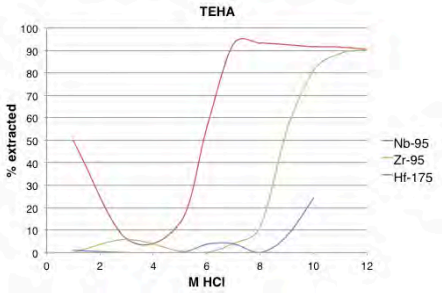

Preliminary data shows a marked separation of zirconium and hafnium. Niobium's extraction is also included as well since it is a decay product of ^{95}Zr. It is important to note that the ^{95}Zr used has stable carrier added to it, so its results cannot be directly correlated to the chemical behavior of single atoms due to the amount of Zr polynuclear species formed.

Goals

For the rutherfordium work, the new ligands mentioned will be tested using ^{89}Zr, ^{95}Zr, and ^{175}Hf by performing solvent extractions with hydrochloric acid. In addition, the dicyclo-18-crown-6 will tested with nitric and sulfuric systems.

If the kinetics are fast, then synthesizing a resin for extraction chromatography and conducting batch studies will be the next step. If any of these extraction system appears show promise, then it will be tested at Texas A&M's cyclotron using short-lived isotopes of zirconium and hafnium. Finally, it will be applied to the study of rutherfordium.

Acknowledgements

This material is based upon work supported by the U.S. Department of Homeland Security under Grant Award Number, 2012-DN-130-NF0001-02.

The views and conclusions contained in this document are those of the authors and should not be interpreted as necessarily representing the official policies, either expressed or implied, of the U.S. Department of Homeland Security.

Prepared by LLNL under Contract DE-AC52-07NA27344

References

1) R. Sudowe, *et al. R. Acta.* **94** (2006) 123–9
2) R. Banda, *et al. J Rad Nucl Chem.* (2013) 13-18
3) R. Wolf , *et al. Inorg. Synth.* **25** (1989) 123-6

IM: LLNL-POST-641875

Lawrence Livermore National Laboratory

Glenn T. Seaborg Institute

Using Computed Tomography to Non-Destructively Characterize Radioactive Fallout in 3D

Rodrigo N. Tapia, B. H. Isselhardt, K. B. Knight, J. D. Sain, I. D. Hutcheon

The University of Georgia

Goal: Develop method to analyze 3D density distributions of fallout provided by computed tomography (CT). In particular, exploring the correlation of X-ray attenuation with average electron density.

Overview:

This project is divided into two main objectives: the exploration of compositional analysis by density mapping and the quantification of void spaces within fallout spheres using CT. Fallout glasses are the resulting debris formed from the rapid vaporization and condensation of ground and device materials during a nuclear detonation.

Why: Void Analysis
- Rapid heating and cooling causes vesicles
- Vesicles are formed by gases that do not fully evolve
- Statistical distributions can help describe timeframe of formation

Why: Density Mapping
- CT provides a 3D density map related to X-ray attenuation
- Greater attenuation is displayed as higher intensity
- X-ray attenuation is correlated to average electron density
- Average electron density is a function of density and atomic number
- This correlation has potential to identify compositions of interest

How CT it Works

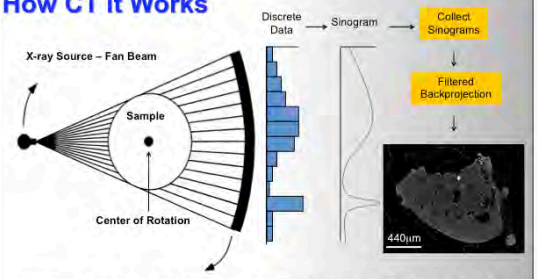

Rotating sample is irradiated by Bremsstrahlung X-ray source. The transmitted X-rays are detected on a CCD array at 360°rotation. Internal structure is reconstructed based on X-ray attenuation at various angles.

Sample mounting

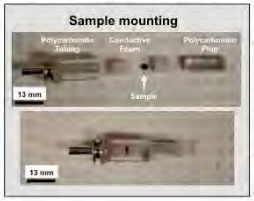

3D Image Data
- Maximum X-ray energy ranged 70-80kV
- Reconstructed data provides images with associated 3D units
- Voxels are the 3D analog for pixels
- Pixel dimension ranged 1.178-2.661μm
- Field of view ~5mm

Results: Density Analysis

Analysis of Localized Inclusions

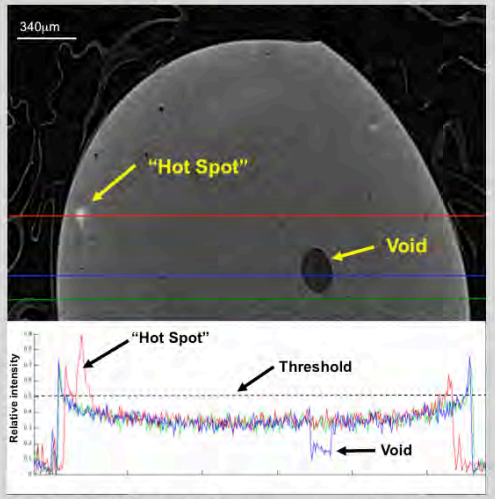

- This is one frame in the 3D reconstruction of Sample 1
- Threshold values are selected just above glass intensity
- Background corrections are made and only hotspots remain
- After threshold selection, hotspots are quantitatively analyzed

Localized Hotspots of High Attenuation

	Material	Mean Intensity	Linear Attenuation Coefficient Normalized to Glass
Sample 1	Glass	0.4079	N/A
	Hotspot 1A	0.8094	0.6853
	Cold Spot	0.3335	-0.2014
Sample 3	Glass	0.3670	N/A
	Hotspot 3A	1.6739	1.5175
	Hotspot 3B	2.3276	1.8472
	Hotspot 3C	2.7638	2.0190

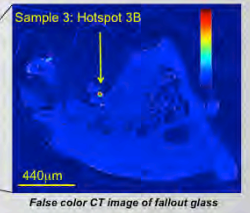

False color CT image of fallout glass

Results: Void Analysis

Developed void isolation algorithm:
1. Isolated volumes of low attenuation
2. Reduced noise and established thresholds to identify voids
3. Calculated void volume and statistics

Void isolation process

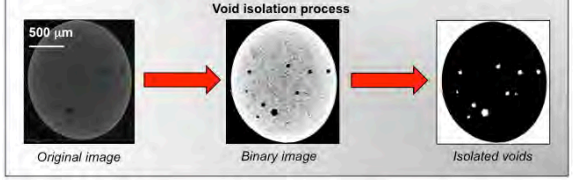

Volume Distribution of Voids

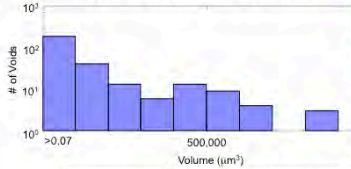

Sample 1 Voids (larger than 0.07μm³)	
Number of Voids	746
Void/Glass Volume	1%
Average Volume (μm³)	8.62E+04
Min Volume (μm³)	1.88E+03
Max Volume (μm³)	5.40E+06

Histogram of void volumes in Sample 1 for voids larger than 0.07μm³. Bin width: 100,000μm³. Total volume of the sphere: 6.33x10⁹μm³.

Conclusions:
- We can spatially resolve objects on the order of 10 microns
- Average electron density and X-ray attenuation are correlated
- We can locate high density inclusions in fallout
- Beam hardening does not significantly impact relative intensity
- Distributions of voids may inform time-temperature sample history

Future Steps:
- Compute 3D maps of fallout features
- Perform CT analyses on 5 additional fallout samples
- Analyze a set of 4 standard metals with CT (Ta, Co, In, Al)
  - Construct a calibration for density vs. attenuation
- Study the relationship between attenuation and composition in fallout
- Analyze hotspots by scanning electron microscopy

Acknowledgements:

This research was performed under the Nuclear Forensics Undergraduate Scholarship Program, which is sponsored by the U.S. Department of Homeland Security, Domestic Nuclear Detection Office and the U.S. Department of Defense, Defense Threat Reduction Agency. This material is based upon work supported by the U.S. Department of Homeland Security under Grant Award Number, 2012-DN-130-NF0001-02. The views and conclusions contained in this document are those of the authors and should not be interpreted as necessarily representing the official policies, either expressed or implied, of the U.S. Department of Homeland Security.

This work was performed under the auspices of the U.S. Department of Energy by Lawrence Livermore National Laboratory under Contract DE-AC52-07NA27344. This work was funded by the Laboratory Directed Research and Development Program at LLNL under project tracking code 10-SI-016. **LLNL-POST-641743**